Available online at www.sciencedirect.com
ScienceDirect
Acta Biomaterialia 4 (2008) 597–612
Acta BIOMATERIALIA
www.elsevier.com/locate/actabiomat

Constitutive modeling of the stress–strain behavior of F-actin filament networks

Jeffrey S. Palmer [a,b,*], Mary C. Boyce [a]

[a] Department of Mechanical Engineering, Massachusetts Institute of Technology, 77 Massachusetts Avenue, 5-017, Cambridge, MA 02139, USA
[b] MIT Lincoln Laboratory, Lexington, MA 02420, USA

Received 28 August 2007; received in revised form 17 November 2007; accepted 18 December 2007
Available online 8 January 2008

Abstract

The central role of the cytoskeleton in both healthy and diseased cellular functions makes it a compelling subject for detailed three-dimensional (3D) micromechanical modeling. Microstructural features of the cytoskeleton govern the cell's mechanical behavior in many of the regulating cellular functions including cell division, adhesion, spreading, migration, contraction, and other mechanotransductive effects which influence biochemical processes. Actin microfilaments (AF) combine to form one of the predominant cytoskeletal networks important to these biological processes.

Here, the AF cytoskeletal microstructure and stress-strain behavior is modeled via a microstructurally-informed continuum mechanics approach. The force-extension behavior of the individual filaments is captured using the MacKintosh derivation of the worm-like chain (WLC) constitutive relationship for short chains where a new and direct analytical expression for the filament force as a function of filament extension is developed in this paper. The filament force-extension behavior is then used in conjunction with the Arruda-Boyce eight-chain network model to capture the 3D multiaxial stress-strain behavior of the network. The resulting 3D cytoskeletal network constitutive model provides the ability to track microstructural stretch and orientation states during 3D macroscopic stretching conditions. The non-affine nature of the network model effectively accommodates the imposed macroscopic shear strain through filament rotation and a relatively small amount of filament stretch. These characteristics enable the network model, using physically realistic material properties, to capture the initial stiffness of the AF network as well as the nonlinear strain stiffening observed at large stresses. The network model predictions compare favorably with published microrheological data of in vitro AF networks.

1. Introduction

Many important biological cellular functions rely on the micromechanics of the cell and its cytoskeleton. The cell's cytoskeletal microstructure performs a crucial role in many of the regulating cellular functions, including cell division, adhesion, spreading, migration, contraction [1] and other mechanotransductive effects which influence many biochemical processes [2].

Actin microfilaments (AF) are one of the primary protein filament components of the cytoskeleton. Microrheological experiments have been conducted on in vitro reconstituted actin networks, quantifying their detailed mechanical behavior (e.g. force deformation, shear frequency, shear concentration) [3,4]. The rheology of cross-linked in vitro AF networks has also been examined [5,6]. These data quantify key features of the mechanical behavior of actin networks needed to develop constitutive models.

1.1. Background on cytoskeletal actin filament networks

Cytoskeletal filamentous actin (F-actin) has an overall diameter of ~7 nm, in vivo contour lengths of ~1 μm [7]

* Corresponding author. Address: Department of Mechanical Engineering, Massachusetts Institute of Technology, 77 Massachusetts Avenue, 5-017, Cambridge, MA 02139, USA. Tel.: +1 781 981 2532; fax: +1 781 981 5398.
E-mail address: jspalmer@mit.edu (J.S. Palmer).

1742-7061/$ - see front matter © 2008 Acta Materialia Inc. Published by Elsevier Ltd. All rights reserved.
doi:10.1016/j.actbio.2007.12.007

and in vitro contour lengths up to 20 μm [8]. The persistence length is defined as $l_p = \kappa/(k_B T)$, where κ is the bending stiffness of the filament, k_B is Boltzmann's constant and T is the absolute temperature. The persistence length of F-actin has been obtained from many experimental techniques, including dynamic light scattering, microscopic observation of thermal fluctuations and microscopic observation of driven oscillation of labeled AF [1]. Typical in vitro measured values of actin filament persistence length, including these and other measurement techniques, range from 3–17 μm [8–16]. Fluorescently labeled AF have been shown to exhibit twice the persistence length of native AF [16], which explains some of the disparity in published values [1]. The force–extension response is usually characterized by a linear region followed by a nonlinear region of increasing tangent stiffness as the filament's extensional limit is reached [7,17].

In vitro rheological experiments on reconstituted actin gel-like networks have been conducted with varying levels of actin and cross-link concentrations [4,5,18–20]. The measured in vitro shear moduli have ranged from 0.01 Pa to several tens of Pa for the same gel concentration, with much of the variation attributed to differences in gel preparation, polymerization and storage in addition to the measurement method chosen [21]. Storage shear moduli of semidilute in vitro networks have exhibited a plateau region at intermediate frequencies (corresponding to time scales of importance to the cell) which is independent of frequency and governed by cross-link interactions [1].

The influence of cross-links in actin networks has been examined by tuning the degree of filament cross-linking and bundling by varying the concentration of cross-links (c_{CL}) for a fixed actin concentration (c_{AF}) or a fixed $R = c_{CL}/c_{AF}$. Using scruin as the cross-linker, Gardel et al. observed in vitro actin–scruin gels exhibiting network behavior for $c_{AF} \geqslant 8$ μM and $R \geqslant 0.03$, and significant bundling effects for $R \sim 0.5$ [22]. For example, the results show the initial shear modulus (G_0) exhibits power-law relationships with actin concentration when $R \geqslant 0.03$: in particular, $G_0 \sim c_{AF}^{2.5}$ for $R = 0.13$ and $G_0 \sim c_{AF}^{2.1}$ for $R = 0.03$ (for $c_{AF} \geqslant 8$ μM) [22].

1.2. Background on cytoskeletal actin network modeling

There have been a number of approaches to modeling isolated homogeneous F-actin networks, including cellular solid models and biopolymer models. The cellular solids model was originally developed by Gibson and Ashby [23] and extended to actin networks by Satcher and Dewey [24]. It describes the cytoskeletal network using a cubical frame with an overall network modulus based on solid fraction (ϕ_s) and deformation of the cell edges. For small ϕ_s, the effective elastic modulus is proportional to ϕ_s if stretching of the edges accommodates the imposed deformation, or ϕ_s^2 if bending and torsion of the edges are dominant [25,26].

The biopolymer models extend polymer theory to biological macromolecules to create biopolymer network models. Polymers are traditionally considered to be flexible if their persistence length is much less than their contour length ($l_p \ll L_c$) and stiff if the opposite is true ($l_p \gg L_c$) [27]. The intermediate regime of semiflexible filaments, in which $l_p \sim L_c$, describes the behavior of many biologically important macromolecules, including F-actin filaments [19]. Accordingly, biopolymers behave more like continuously flexible filaments rather than the traditional polymer theory of freely jointed chains of rigid rods [1]. The Kratky–Porod [28] based worm-like chain (WLC) model provides a representation of the axial extension of flexible filaments and is derived from the free energy of bending deformation due to thermal fluctuations. As the filament is stretched, the amplitude of the undulations decreases. This decrease in thermal undulation amplitude results in a corresponding decrease in available filament conformations, leading to a decrease in entropy and an increase in the axial stiffness of the flexible filament. The WLC model has been effective at describing the entropic elasticity of a number of single molecules when $L_c \gg l_p$, including DNA at low to moderate strains [29]. Although its force–extension relationship requires numerical evaluation of the path integral, interpolation formulas have been successfully used to simplify calculations (e.g. [30]). Subsequent molecular theories (e.g. [19]) have addressed the semiflexible regime for $L_c \sim l_p$ with energy functionals and force–deflection relationships that are still entropic in origin. For extensions where the filament end-to-end distance approaches the contour length, the entropic-based force–deflection relationships for the flexible and semiflexible filaments have been expanded to include an additional term for the enthalpic axial stretch contribution [31–33].

Biopolymer network models calculate the elastic properties of cytoskeletal networks by incorporating the force–deflection behavior of individual elastic cytoskeletal filaments within models of the network geometry [3,19,20,34–36]. This also provides a framework for determining the effect of cross-linking proteins on the behavior of cytoskeletal filament networks. Empirically observed shear moduli for F-actin networks with permanent cross-links (but the same concentration of F-actin) have been observed to vary over two orders of magnitude by varying the cross-link density [22].

In order to determine the network elastic properties, biopolymer models often employ a three-dimensional (3-D) volume averaged framework of the 1-D filament force–extension response by taking a chain aligned in the primary load direction to govern the network behavior (see Fig. 1a) [3,19]. These models often assume affine network deformation [20], and can further be constructed to account for varying degrees of cross-link densities. For the limit of maximum cross-link density the shear modulus is related to the solid fraction as $G \sim \phi_s^{5/2}$ [37].

Although successful in capturing some scaling relationships (such as cross-link density effects), depending on the

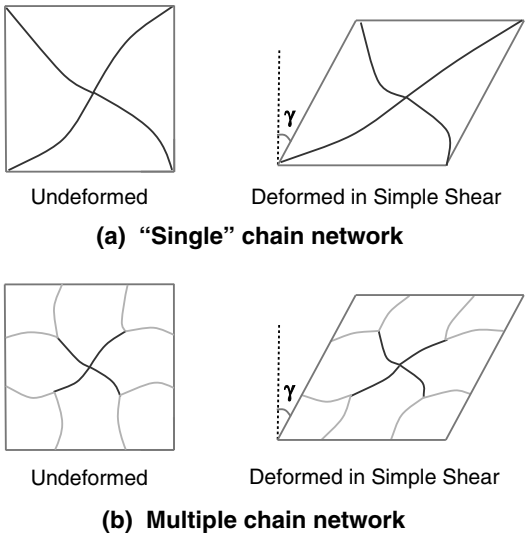

Fig. 1. Comparison of two network structures (a) and (b) in their undeformed states (left) and after deformation by simple shear (right). Network (a) approximates network behavior based on a chain aligned with the maximum principal stretch direction and network (b) considers a simple multiple chain network geometry, illustrating how deformation is accommodated in a non-affine manner primarily through chain rotation with relatively little chain stretch (compared with case (a) above).

network topology, network models can inadvertently overweigh the contributions of chains aligned in a primary load direction. As a simple example, Fig. 1a depicts a network subject to simple shear where the network shear strain is accommodated by extensive chain stretching of chains along the diagonal (the initial principal stretch direction) with relatively modest rotation of the constituent chains. Real network structures will accommodate the macroscopic deformation with constituent chains undergoing both rotation and stretch. Indeed, much of the imposed deformation will be accommodated by chain rotation with a relatively small amount of chain stretch. For comparison purposes, the deformation of the network depicted in Fig. 1a is contrasted to an alternative simple network shown in Fig. 1b. For the network of Fig. 1b, the imposed shear strain is primarily accommodated by the rotation of the constituent chains with relatively little chain stretch, especially as compared with the network deformation of Fig. 1a. Hence, more realistic cytoskeletal network models must address the network's ability to accommodate deformation by both rotation and stretching (where the minimum energy configuration that satisfies compatibility and equilibrium will be found by the network).

Random networks, averaging over the contributions of all chain orientations but taking an affine mapping of the macroscopic deformation to all chains, have been employed to model polymer network deformation as introduced by Treloar and Riding [38] and further pursued by Wu and van der Giessen [39]. Recently this same approach has been applied to the rheology of biopolymer networks [20]. Averaging over all chain orientations begins to capture the contributions of rotation and stretching, but the affine deformation assumption results in the direct stretching of chains aligned with a primary stretch direction, and these chains then dominate the macroscopic stress–strain prediction. Some biopolymer networks, such as the spectrin cytoskeletal network of the red blood cell, have a well-defined triangulated geometry which has been modeled using the freely jointed chain model [34,35] as well as the WLC model [40–42] to capture chain behavior together with kinematically prescribed mapping of the macroscopic deformation to the representative triangular network unit cell.

In this paper, the single filament models will be integrated into the Arruda–Boyce eight-chain network model [43], which accommodates the stretch and orientation states of isotropic, randomly oriented chain networks in a simple averaged manner. The 3-D network model will be adjusted to include the effects of bundling on structure and mechanical behavior. Once the constitutive model has been established, it will be compared with the experimental data of Gardel et al. [22] discussed earlier.

2. Actin network constitutive model description

Here, we propose a constitutive model for the stress–strain behavior of the cytoskeletal AF network. The force–extension behavior of the AF will be taken to follow a MacKintosh-type model. The AF network will be modeled as an effective eight-chain network to capture the molecular network structure.

2.1. Single filament model

Following the Kratky–Porod formulation [28], the MacKintosh model is derived from the total energy of bending deformation due to thermal fluctuations [28]:

$$E_{K-P} = \frac{\kappa}{2}\int_0^{L_c} (\partial\vec{t}/\partial s)^2 \, ds \tag{1}$$

where $\vec{t}$ is the unit tangent vector of any point along the arc length, s, on a curved filament of contour length L_c (Fig. 2).

The MacKintosh model [19,44] describes a filament at a finite temperature, with transverse thermal fluctuations that result in a contraction, $(\Delta L)_{F=0}$ in Fig. 2, causing the

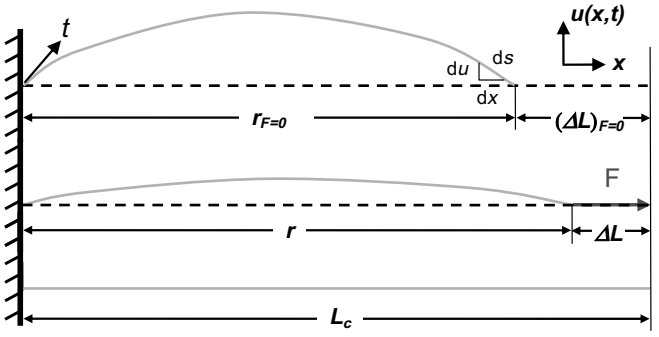

Fig. 2. Single filament schematic (adapted from Ref. [44]).

end-to-end distance, r, at an axial force, F, of zero to be less than the filament contour length, $r_{F=0} = L_c - (\Delta L)_{F=0}$. Letting the x-axis define the average orientation of the filament and u define one of the two transverse displacements, the total energy associated with applying a force (F) to extend the filament can be shown to be

$$E_{Total} = \frac{1}{2}\int_0^{L_c}\left[\kappa\left(\frac{\partial^2 u}{\partial x^2}\right)^2 + F\left(\frac{\partial u}{\partial x}\right)^2\right]^2 dx \quad (2)$$

This equation can be solved using a Fourier series with pinned boundary conditions along with the theory of equipartition of energy [44]. Based on the equilibrium amplitudes, the contraction (for small transverse fluctuations) must satisfy

$$\langle \Delta L\rangle = L_c - r = \frac{L_c^2}{l_p \pi^2}\sum_n \frac{1}{(n^2+\phi)} \quad (3)$$

where the dimensionless force $\phi = FL_c^2/\kappa\pi^2$, and a factor of two is included to account for the two transverse degrees of freedom of a filament in 3-D fluctuation [44]. The nonzero value of r at the zero force condition, important for network calculations, is then found directly from

$$\langle \Delta L\rangle_{\phi=0} = L_c - r_{F=0} = \frac{L_c^2}{6l_p} \Rightarrow r_{F=0} = L_c\left(1 - \frac{L_c}{6l_p}\right) \quad (4)$$

We simplify the series relation of Eq. (3) through the use of the Langevin function. The series for the average contractions converges to the following expression:

$$\langle \Delta L\rangle = L_c - r = \frac{L_c^2}{l_p\pi^2}\left(\frac{\pi\sqrt{\phi}\coth(\pi\sqrt{\phi}) - 1}{2\phi}\right) = \frac{L_c^2}{2l_p}\left[\frac{\mathscr{L}(\pi\sqrt{\phi})}{\pi\sqrt{\phi}}\right] \quad (5)$$

where $\pi\sqrt{\phi} = L_c\sqrt{F/\kappa}$ and $\mathscr{L}(\beta)$ is the Langevin function defined by $\mathscr{L}(\beta) = \coth(\beta) - 1/\beta$.

Since the functional dependence of F on r is of more interest than r as a function of F, Cohen's Padé approximation for the inverse Langevin equation [45],

$$\mathscr{L}^{-1}(x) = x\frac{3-x^2}{1-x^2} + O(x^6) \quad (6)$$

is used to create a more useful force–extension relationship,

$$F_{Mac} = \frac{k_B T}{l_p}\left(\frac{1}{4(1-r/L_c)^2}\right)\left(\frac{L_c/l_p - 6(1-r/L_c)}{L_c/l_p - 2(1-r/L_c)}\right) \quad (7)$$

which reduces to Eq. (4) for the zero force condition. This approximation is valid for tensile and compressive forces subject to $(1 - 0.3L_c/l_p) < r/L_c < 1$; noting that $r_{F=0}/L_c = 1 - 0.167L_c/l_p$, this approximation covers the range of filament extension of relevance for the semiflexible ($l_p \sim L_c$) network. In order to maintain a positive extension, $r/L_c > 0$, the approximation is therefore subject to the following limits for tensile loads ($L_c < 6.0l_p$) and compressive loads ($L_c < 3.3l_p$). The Padé approximation-based force–extension expression, Eq. (7), compares very favorably with the exact numerical expression, Eq. (3), with the average error for each of the four cases in Fig. 3a ($l_p = 3,\ 5,\ 7.5,\ 10\ \mu m$) equal to 0.4%, 0.8%, 1.2% and 1.5%, respectively.

Fig. 3a shows the single filament response of the MacKintosh model using characteristic properties of F-actin filaments from a densely cross-linked network ($l_p = 3$–$10\ \mu m$, $L_c = 1\ \mu m$). The end-to-end distance at zero force, $r_{F=0}$, depends strongly on the combination of persistence length l_p and contour length L_c. Here, keeping L_c constant and varying l_p from 3 to 10 μm, we see the effect of l_p on $r_{F=0}$ at the different starting points of Fig. 3a, where $r_{F=0}$ is smaller for smaller l_p. This then results in the increased initial chain stiffness with increasing l_p, as shown in Fig. 3a. Note that a densely cross-linked network ($l_p > L_c$) operates in this highly nonlinear regime of the force–extension curve

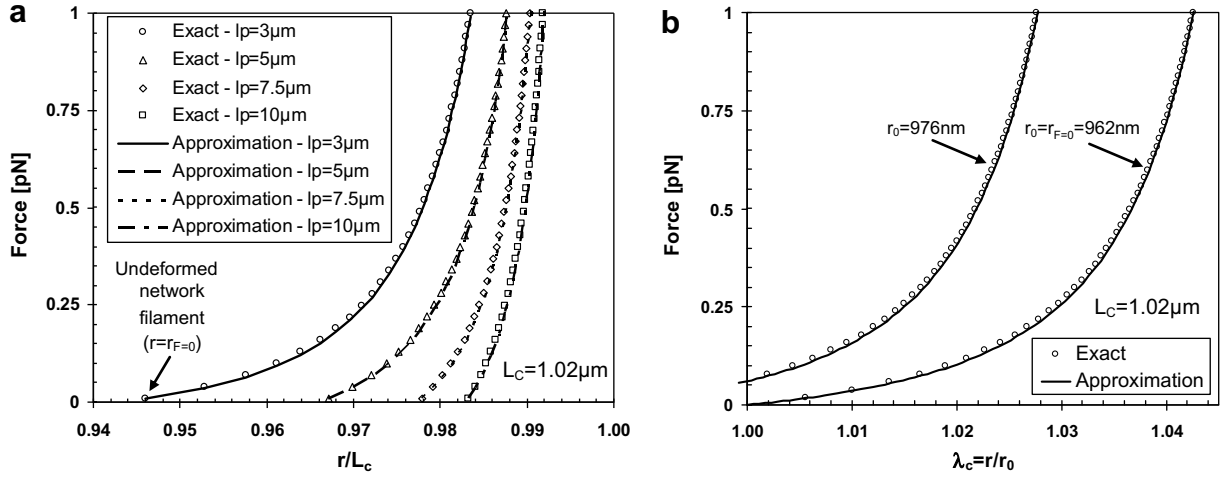

Fig. 3. (a) The effect of persistence length on filament force–extension behavior as computed using the MacKintosh model (fixing contour length to $L_c = 1.02\ \mu m$); (b) the effect of pretension on filament force–stretch behavior as computed using the MacKintosh model (for the case of $L_c = 1.02\ \mu m$; $l_p = 3\ \mu m$). Both figures show exact results as well as results using the proposed approximation (Eq. (7)), illustrating the accuracy of the approximation.

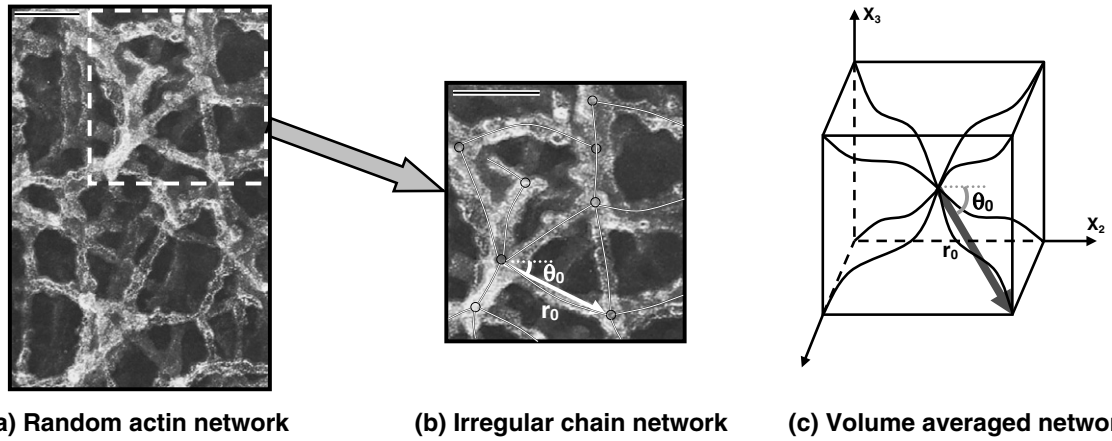

Fig. 4. Random F-actin network and corresponding idealized eight-chain network model. The stereomicrograph of the actin cortex is adapted from Ref. [58]. J Cell Biol. Copyright 1983 The Rockefeller University Press. The bar in (a) and (b) is 0.1 μm.

(i.e. $r/L_c > 0.94$ in Fig. 3a). Fig. 3b shows the effect of a different initial end-to-end distance, r_0, on the filament force–stretch ($\lambda_c = r/r_0$) behavior. Here, taking the case of $l_p = 3$ μm and $L_c = 1.0$ μm, which has a zero force length of $r_{F=0} = 0.962$ μm, we compare the behavior when $r_0 = r_{F=0} = 0.962$ μm to that when $r_0 = 0.976$ μm. The $r_0 = 0.976$ μm case begins with an initial tensile force on the filaments (i.e. chain pretension) of $F_0 = 0.07$ pN. The pretension results in the observed increase in initial stiffness and decrease in limiting stretch shown in Fig. 3b. Conversely, a precompression condition will shift the curve to the right, resulting in a lower value on the ordinate axis, a reduced initial stiffness and an increased limiting stretch.

2.2. Network model

A network structure can be described by four basic topological features (see Fig. 4): (i) a distribution in the initial distance between network junctions, which we call the junction-to-junction distance or initial filament length, r_0; (ii) a distribution in the fully extended length (i.e. contour length) of a filament between network junctions, L_c; (iii) the network connectivity (functionality of network junctions); and (iv) the orientation distribution of the filaments. In order to simplify the mathematical description of the network structure, we will represent these basic features of the network in terms of average or idealized quantities: (i) an average initial filament length; (ii) an average filament contour length; (iii) an idealized network connectivity; and (iv) the average orientation of the filaments. We further simplify to the case of an initially isotropic network (no preferred orientation in the initial state).

The orientation of a filament can be defined by the angle between a reference axis and the junction-to-junction vector connecting the ends of the filament. For an initially isotropic network, filaments are randomly oriented in space. Thus, the average filament angle can be obtained by taking the volume average of all possible orientations, and is given by

$$\langle\theta\rangle = \int_{\alpha_s=0}^{\pi/2} d\alpha_s \int_{\beta_s=0}^{\pi/2} d\beta_s \cos^{-1}[\cos\alpha_s \cos\beta_s]\cos\alpha_s = 57.3^\circ$$

where α_s and β_s are the azimuthal and polar angles, respectively, in the spherical coordinate system (see [46] for the analogous case of molecular orientation in polymeric networks). An alternative average can be obtained using Hermann's orientation function and gives 54.7°. Therefore, an idealized network topology should capture an initial average filament orientation close to that of 54–57°.

An idealized network structure that has been found to capture this initial orientation in an average sense is the eight-chain network model of Arruda and Boyce, which was originally proposed to capture 3-D aspects of macromolecular network structure and its evolution with deformation in elastomeric [43] and glassy thermoplastic [47] materials. A combined WLC/eight-chain model has also been extended to anisotropic biopolymer networks, such as the collagen network in skin tissue by Bischoff et al. [48] and Kuhl et al. [49], and an isotropic eight-chain network model of unfolding modular chains developed by Qi et al. [36]. Bertoldi and Boyce extended both of these models to capture the behavior of mussel byssus via an anisotropic eight-chain network model with a filament model that captures the straightening out of bends in byssus molecular chains using an elastica-type solution followed by axial stretching of the chains and subsequent force-induced unfolding of the modular domains [50]. Here, we apply the eight-chain network approach to densely cross-linked and bundled cytoskeletal networks in which $L_c < l_p$. The eight-chain network considers an averaged or idealized structure of eight chains located along the diagonals of a cubic unit cell and connected by a centrally located junction (see Fig. 5). For the isotropic network, the cell is taken to be aligned with and to deform with the macroscopic principal stretches. Therefore, taking the normal to any face of the cell as the reference axis, the average initial chain orientation of this network is simply the initial orientation of the eight chains or 54.7°, capturing

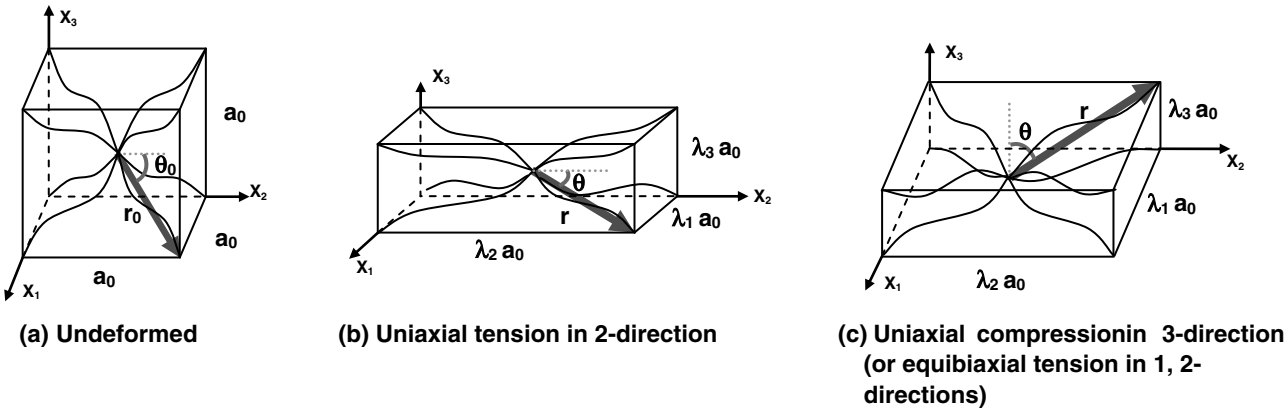

Fig. 5. Eight-chain network model geometry and deformation (adapted from Ref. [43]).

the average orientation for a randomly oriented network. Since the cell deforms with the principal stretch state λ_i (where i represents the three principal directions), the stretch on any chain in this network, λ_c, is the root-mean square of the principal stretches and is always tensile for isochoric deformations,

$$\lambda_c = r/r_0 = \sqrt{(\lambda_1^2 + \lambda_2^2 + \lambda_3^2)/3} = \sqrt{I_1/3}$$

where $I_1 = \lambda_1^2 + \lambda_2^2 + \lambda_3^2$ is the first invariant of the left or right Cauchy–Green tensor. The initial end-to-end distance is related to the network's actin concentration (c_{AF}) and filament properties (L_c, l_p). The chains are also found to rotate towards the maximum principal stretch direction(s). For example, in the case of uniaxial tension, the chains extend and rotate towards the tensile axis (Fig. 5b); in the case of uniaxial compression (or equibiaxial tension), the chains extend and rotate away from the compression axis (Fig. 5c). For the cases of uniaxial tension and uniaxial compression, the principal axes remain fixed throughout the deformation, and thus the chains in the unit cell rotate and stretch in an affine manner.

The "non-affine" mapping of macroscopic deformation to network chain deformation is more apparent when examining the case of simple shear (see Fig. 6). The macroscopic basis is denoted as $\{xyz\}$, while the principal basis is shown as $\{123\}$. In the undeformed state, the principal basis is undefined and could be oriented in any direction (see Fig. 6a). Upon application of simple shear, the principal axes of stretch are identified and will rotate with deformation and, furthermore, the chains will undergo additional rotation relative to the maximum principal stretch direction (θ_1; see Fig. 6b). Hence, this network representation is seen to accommodate the imposed shear by both non-affine rotation and non-affine stretching of the constituent chains, effectively sampling the non-affine nature of the network behavior in a simple but effective manner. The physical counterpart would be to view the rotated unit cell as a method of sampling the rotation and stretching of chains (in eight directions with respect to the maximum principal direction) such that the overall non-affine network response is captured in an averaged sense. The eight-chain network model formulation captures the basic features that Chandran and Barocas [51] and Onck et al. [52] observe in their many membered discrete network modeling approaches, in particular, the significant reorientation of filaments that accommodates macroscopic deformation.

Due to the ability of the eight-chain network to effectively mimic the initial state of a randomly oriented network and to also capture the evolution in chain stretch and orientation with different deformation states, this simplified network topology will be utilized to represent the cytoskeletal network.

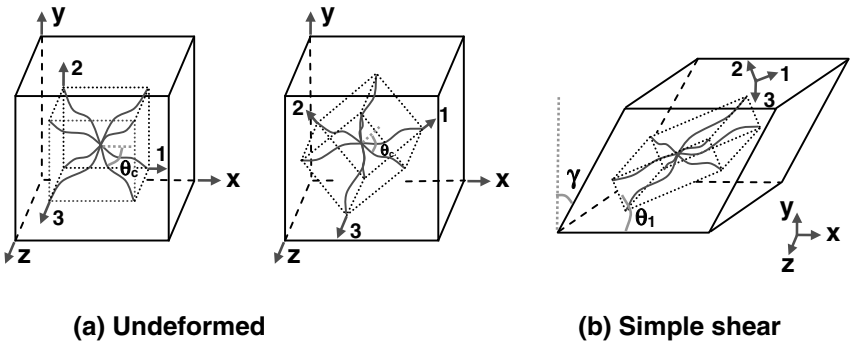

Fig. 6. Simple shear deformation of eight-chain network model.

2.3. Stress–strain behavior

The three-dimensional stress–stretch behavior of the AF network can be determined using the eight-chain network topology and its evolution with stretch together with a representation of the axial force–stretch behavior of an AF where the initial length of the filament is the initial junction-to-junction distance, r_0, and the limiting length is essentially the contour length, L_c, of the filament. Cytoskeletal filaments, especially AF, are observed to have only a slight curvature between junction points (Fig. 4a). The force–extension relations govern the filament's response during axial stretching by displacing the two junction points and thus increasing the junction-to-junction distance from r_0 to r. The force–stretch behavior will consist of an initially linear elastic region, followed by a strain stiffening region as the junction-to-junction distance r approaches the filament contour length L_c (see Fig. 3a). The limiting filament stretch is therefore defined as $\lambda_L = L_c/r_0$.

The work done by each chain can be found by integrating the filament force–extension expression (Eq. (7)):

$$\Delta W_c = \int F \, dr$$

and is equal to the filament strain energy. The strain energy density of the network, U, is simply the product of the filament density, n (number of filaments per unit volume), multiplied by the strain energy of a single filament, u_f, in the eight-filament network: $U = nu_f$ since all filaments in the eight-chain network experience the same stretch. The expression for the strain energy density of the eight-filament cytoskeletal network model is

$$U_{Mac} = \frac{nk_BT}{l_p}\left[\frac{L_c}{4(1-r/L_c)} - l_p[\ln(L_c^2 - 2l_pL_c + 2l_pr) - \ln(r - L_c)] - c\right] \quad (8)$$

where c is a constant equal to the initial strain energy density from the filaments. Since $r = \lambda_c r_0 = r_0\sqrt{I_1/3}$, the strain energy density expression is a function of I_1.

The actin cytoskeleton is embedded in a nearly incompressible fluid (cytosol) and hence is taken to deform at constant volume.[1] The Cauchy stress is found by differentiating the strain energy density:

$$\mathbf{T} = 2\frac{\partial U}{\partial I_1}\mathbf{B} - p^*\mathbf{I} = \frac{nk_BT}{3l_p}\frac{r_0}{\lambda_c}\left(\frac{1}{4(1-\lambda_c r_0/L_c)^2}\right) \times \left(\frac{L_c/l_p - 6(1-\lambda_c r_0/L_c)}{L_c/l_p - 2(1-\lambda_c r_0/L_c)}\right)\mathbf{B} - p^*\mathbf{I} \quad (9)$$

where $\mathbf{B} = \mathbf{F}\mathbf{F}^T$ is the left Cauchy–Green tensor (Finger tensor), $\lambda_c = \sqrt{\mathrm{tr}(\mathbf{B})/3}$ and the deformation gradient $\mathbf{F} = \partial \boldsymbol{x}/\partial \boldsymbol{X}$, where $\boldsymbol{x}$ is the position vector of a material point in the current configuration and $\boldsymbol{X}$ is the original position. Also in Eq. (9), $\mathbf{I}$ is the identity tensor and p^* is the additional pressure required due to the incompressibility constraint and obtained by satisfying equilibrium. The Cauchy shear stress–strain relationship becomes

$$\tau_{Mac} = \frac{nk_BT}{3l_p}\frac{r_0}{\lambda_c}\left(\frac{1}{4(1-\lambda_c r_0/L_c)^2}\right) \times \left(\frac{L_c/l_p - 6(1-\lambda_c r_0/L_c)}{L_c/l_p - 2(1-\lambda_c r_0/L_c)}\right)\tan\gamma \quad (10)$$

The initial shear modulus is given by

$$G_0 = \frac{nk_BTr_0}{3l_p}\left(\frac{1}{4(1-r_0/L_c)^2}\right)\left(\frac{L_c/l_p - 6(1-r_0/L_c)}{L_c/l_p - 2(1-r_0/L_c)}\right) \quad (11)$$

The constitutive model presented here is a function of the material properties n, l_p, L_c and r_0. The filament density, n (filaments m^{-3}), is defined as $n = \rho_L/L_c$. The actin length density, ρ_L (μm m^{-3}), is defined as $\rho_L = (c_{AF} \cdot M_{AM})/\rho_{AF}$ where c_{AF} is the experimental actin monomer concentration, ρ_{AF} (Da μm^{-1}) is the linear actin density and M_{AM} (Da monomer^{-1}) is the molecular mass of each actin monomer. Both ρ_{AF} and M_{AM} are actin material properties, defined a priori. As defined earlier, the zero force junction-to-junction distance $r_{F=0}$ is a function of L_c, l_p, where a network initial junction-to-junction distance r_0 slightly larger than $r_{F=0}$ indicates a prestress in the network due to in vitro or in vivo environmental conditions [17,53,54]. Here, the percent increase (α) of r_0 beyond $r_{F=0}$ is defined as $r_0 = r_{F=0}(1+\alpha)$. In principle, r_0 and L_c are measurable from micrographs and l_p is measurable from single molecule bending; however, they are operationally fit from empirical stress–strain data for each network.

3. Actin filament network constitutive model results

3.1. Experimental data used for comparison

The rheology of actin networks has been quantified in several studies [3,6,10,22,55]. We will compare our model to the Gardel et al. data [22] which systematically varied c_{AF} while holding $R = c_{CL}/c_{AF}$ constant. This data measured the shear rheology of F-actin cross-linked with scruin cross-linking proteins.

3.2. Representative low concentration case

The model was evaluated by first fitting the model to the data with the lowest actin concentration found to exhibit entangled network behavior, $c_{AF} = 8$ μM and $R = 0.03$. The contour length was calculated following the relation presented by Gardel et al. [22] and the empirically derived exponent (0.2) given by Shin et al. [4] for actin–scruin networks,

[1] Note that this network model can be incorporated into poroelastic frameworks to capture fluid flow and, consequently, swelling/deswelling effects on the behavior.

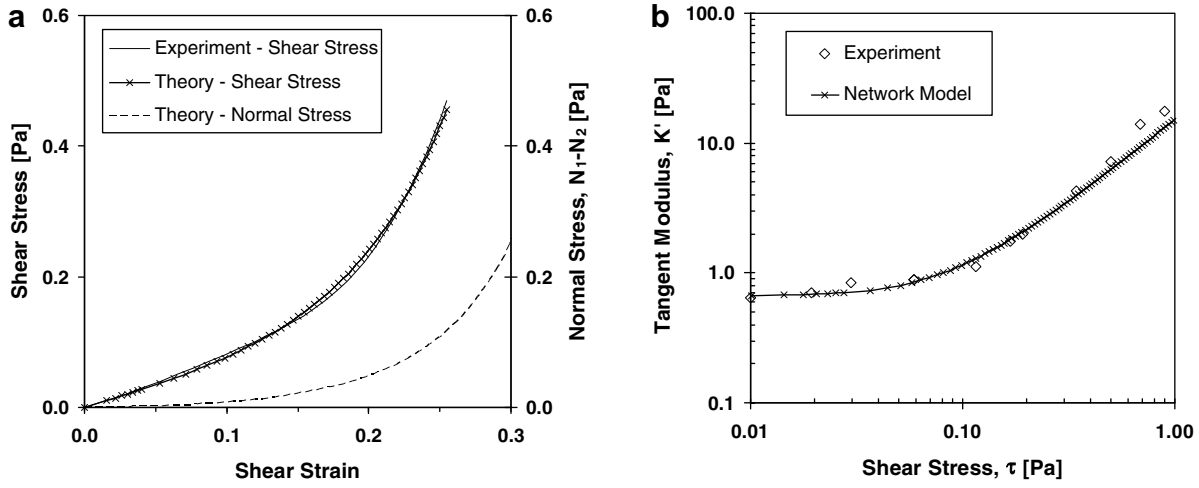

Fig. 7. (a) Shear stress and normal stress difference ($N_1 - N_2$) vs. shear strain and (b) tangent shear modulus vs. shear stress for in vitro F-actin networks ($c_{AF} = 8$ μM, $R = 0.03$). The experimental data are adapted from Ref. [22].

$$L_c = \frac{R^{0.2} d_{Actin}}{2} \sqrt{\frac{\pi}{c_{AF}}} \tag{12}$$

with $d_{Actin} = 7$ nm, $R = 0.03$ and $c_{AF} = 8$ μM, resulting in $L_c = 1.1$ μm. The chain density is determined to be $n = 1.2e19$ filaments m^{-3} based on the values of $L_c = 1.1$ μm, $c_{AF} = 8$ μM, $\rho_{AF} = 16$ MDa μm^{-1} and $M_{AM} = 42$ kDa monomer^{-1}. The values of l_p and α are chosen to best fit the model to the 8 μM experimental data, noting that the value of r_0 associated with α will be nearly equal to L_c based on the observed network topology of nearly straight filaments between junctions. The best fit of $l_p = 3$ μm agrees with observed values of $l_p \sim 3$ μm for F-actin with $L_c \sim 1$–3 μm [16].

The shear stress–strain results are shown in Fig. 7a, with the tangent modulus–shear stress results shown in Fig. 7b. The network modeling parameters are $n = 1.2e19$ filaments m^{-3}, $l_p = 3.0$ μm, $L_c = 1.1$ μm and $r_0 = 1.0$ μm. The network model captures the experimental data through the entire range of shear strain using physically realistic material properties. The network model also fits well with the experimental tangent modulus–shear stress behavior, including the low stress region of relatively stress-independent modulus and the nonlinear increase in tangent modulus at higher levels of shear stress.

The AF network model also enables tracking of the evolution in filament orientation and stretch with macroscopic deformation. The average orientation of a filament is expressed as the azimuthal angle with respect to the direction of maximum principal stretch (θ_f), together with the direction of the maximum principal stretch defined by its angle (θ_1) with respect to the direction of imposed shear (see inset of Fig. 8).

The filament orientation evolution shows that the shear strain is accommodated by significant filament rotation and a small amount of filament stretch. The eight-filament network gives a filament stretch of $\lambda_f = 1.0004$ for a shear strain of $\tan(\gamma) = 0.05$ and $\lambda_f = 1.01$ for $\tan(\gamma) = 0.25$. In contrast, an affine network with a dominating diagonal filament (e.g. Fig. 1a) subjected to shear strains of $\tan(\gamma) = 0.05$ and 0.25 requires much larger filament stretches of $\lambda_f = 1.03$ and 1.15, respectively.

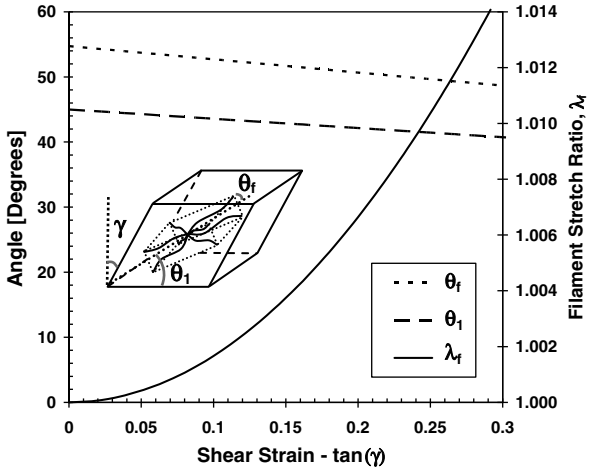

Fig. 8. F-actin filament molecular orientation evolution.

Fig. 7a also shows the normal stress difference, $N_1 - N_2$ (where $N_1 = T_{11} - T_{22}$, $N_2 = T_{22} - T_{33}$) as a function of shear strain during the simple shear deformation. The normal stress difference is found to be negligible at small strains and to increase monotonically as a positive value, as expected, for an initially isotropic network based on the first invariant of strain. Gardel et al. did not present results for the normal stress difference for their networks. However, recent work by Janmey et al. [56] has observed a negative normal stress difference during finite shear of much higher concentration, cross-linked actin networks. This suggests a possible initial anisotropy in the Janmey network configuration which could be modeled using an anisotropic formulation of the eight-chain network (e.g. [57]), or, alternatively suggests a cross-linking condition that favors direct axial stretching of the filament over fila-

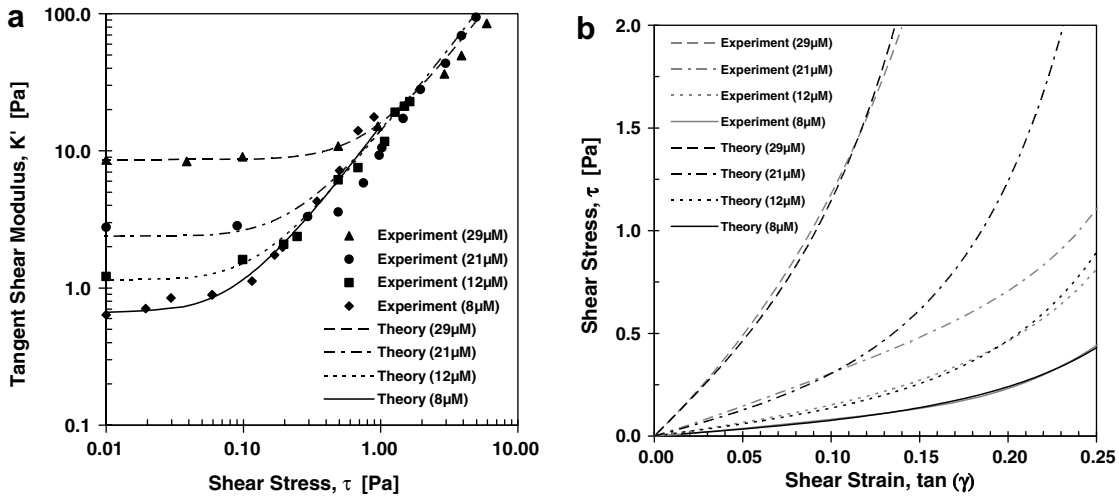

Fig. 9. (a) Tangent shear modulus–shear stress theory and experimental data; (b) shear stress–shear strain theory and experimental curve fit data of actin networks with varying actin concentration ($c_{AF} = 8$, 12, 21, 29 μM, $R = 0.03$). The experimental data are adapted from Ref. [22].

ment rotation; this effect could be captured in future expansions of the strain energy function by including torsional potential contributions of the cross-linking junctions and the enthalpic contributions from direct axial stretching of the chains.

3.3. Effects of increasing actin concentration

Gardel et al. further explored the effects of varying actin concentration and cross-link concentration on the shear rheology of the network. Fig. 9a shows the tangent modulus–stress behavior for four levels of c_{AF} at fixed $R = 0.03$. Note in Fig. 9a that the tangent shear modulus for the $c_{AF} = 21$ μM case is constant up to a shear stress of $\tau = 0.5$ Pa, while the trend of nonlinear strain stiffening observed in the other three concentrations suggests that the 21 μM network should begin strain stiffening at approximately $\tau = 0.2$ Pa. The shear stress–strain data were obtained by taking a curve fit of the raw tangent modulus–stress data to calculate the shear stress–strain behavior. The experimental data in Fig. 9b show the resulting shear stress–strain behavior for varying c_{AF} at fixed $R = 0.03$.

We now explore the ability of the proposed model to capture the effect of actin concentration on the stress–strain behavior by attributing the observed effects to changes in the network structure (n, r_0, etc.). We then evaluate the model's ability to capture network prestress and bundling effects by parametrically changing r_0 and l_p, respectively. We begin by determining l_p, L_c and α (due to prestress) for the lowest concentration case (8 μM) shown previously. The persistence length is then held constant (indicating a "no bundling" assumption), while the contour length is taken to scale with concentration ($L_c \sim c_{AF}^{-1/2}$) following Eq. (12). The percent increase (α) in r_0 beyond $r_{F=0}$ due to prestress for each concentration is then adjusted to provide a fit to the experimental results, as shown in Fig. 9. Table 1 contains the network parameters used for each concentration case, with the initial prestress (σ_0) based on $r_0 = r_{F=0}(1 + \alpha)$.

Note also that α decreases monotonically with $c_{AF} = 8$, 12, 29 μM (ignoring the anomalous 21 μM data), approximately following the relationship $\alpha = 6.2(c_{AF})^{-1/2}$. The stress–strain results correlate well with both the 12 and 29 μM data, as shown in Fig. 9b. The model also captures the experimental behavior for the entire range of applied shear stress, as shown in the originally published log–log plot of tangent modulus vs. shear stress shown in Fig. 9a. The good agreement between the model result and the data also indicates that there is relatively little bundling in these cases, and that the increasing stiffness with increasing c_{AF} is due to the change in network topology. The good agreement in the high stress region, where strain stiffening occurs, is a benefit of using a network model that accounts for the non-affine deformation of a network, accommodating macroscopic deformation by rotation of filaments and a small amount of filament stretch.

Note that the network model results for the 21 μM case in Fig. 9 exhibits the transition to nonlinear strain stiffening behavior by $\tau = 0.2$ Pa, consistent with the empirical trend

Table 1
Network parameters for different actin concentrations

Concentration (μM)	l_p (μm)	n (m^{-3})	L_c (μm)	$r_{F=0}$ (μm)	r_0 (μm)	α (%)	σ_0 (Pa)
8	3.0	1.2e19	1.07	1.00	1.03	2.7	0.66
12	3.0	2.1e19	0.89	0.85	0.87	2.1	1.1
21	3.0	5.1e19	0.67	0.64	0.65	1.2	2.4
29	3.0	8.2e19	0.57	0.55	0.56	1.4	8.6

exhibited by the other concentrations. The network model results for the 21 μM case also exhibit good agreement with the experimental tangent modulus–shear stress data in Fig. 9a in both the low and high stress regions. The 21 μM shear stress–strain predictions of Fig. 9b are in good agreement with the data up to a strain of 0.10, but exhibit a much stiffer behavior at larger strains. This is likely a direct result of the ambiguity of the 21 μM tangent modulus data in the transition region which is key to reconstructing the stress–strain curves.

3.3.1. Parametric evaluation of prestress effects

Prestress occurs in both in vitro or in vivo networks due to a variety of environmental conditions [17,53,54]. In vitro or in vivo actin networks could experience the prestress from sources including osmotic/swelling pressures, external tractions due an adherent cell membrane's interactions with the ECM (or the in vitro gel's interactions with the substrate), and/or internal myosin-generated contractile forces. The proposed eight-chain MacKintosh network model can account for prestress and hence can be used to parametrically explore the effect of prestress on the stress–strain behavior. The actin network prestress is accounted for directly through a percent increase (α) in r_0 beyond $r_{F=0}$. Fig. 10 demonstrates the effect of an increase in network prestress on the overall network shear stress–strain behavior. The results show that increasing prestress results in an increase in the initial shear modulus of the network and a decrease in the network extensibility (as seen in the dramatic increase in tangent modulus (slope) of the stress–strain curve occurring at smaller strains when prestress is increased).

3.3.2. Parametric evaluation of bundling effects

The network will also become stiffer with increasing persistence length. Filament bundling increases the persistence length of the "effective" bundled filament. At large values of R ($R = 1$) the actin network behavior is dominated by thick bundles, in contrast to almost no bundling observed at $R = 0.03$ [22]. Here, we explore the ability of the proposed model to capture the stiffening effects of bundling.

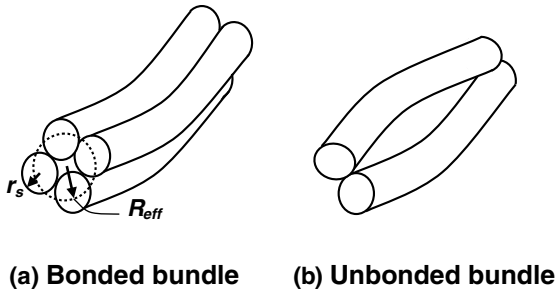

Fig. 11. Filament bundling geometry with (a) bonded bundles and (b) unbonded bundles.

The bending stiffness of the bundle, and hence l_p, can be determined from the number of filaments per bundle (m). Filament bundles might be unbonded, partially bonded along the length or fully bonded along the entire axial length of the filaments. Here we examine the two limiting cases of "unbonded bundles" and fully "bonded bundles". The stiffness of unbonded bundles will scale linearly with the number of filaments in the bundle. The stiffness of bonded bundles will scale by the ratio of the effective moments of inertia of the bonded geometry with that of the single filament; this scaling is determined by estimating the effective bonded bundle radius (R_{eff}).

For bundles with two adjacent filaments ($m = 2$), the stiffness is simply twice the stiffness of an individual filament. For bundles with $m \geqslant 3$, the unbonded bundle stiffness will simply scale linearly with m. For bonded bundles with $m \geqslant 3$, the increase in R_{eff}, which leads to an increase in stiffness from bundling, is illustrated in Fig. 11a (where r_s

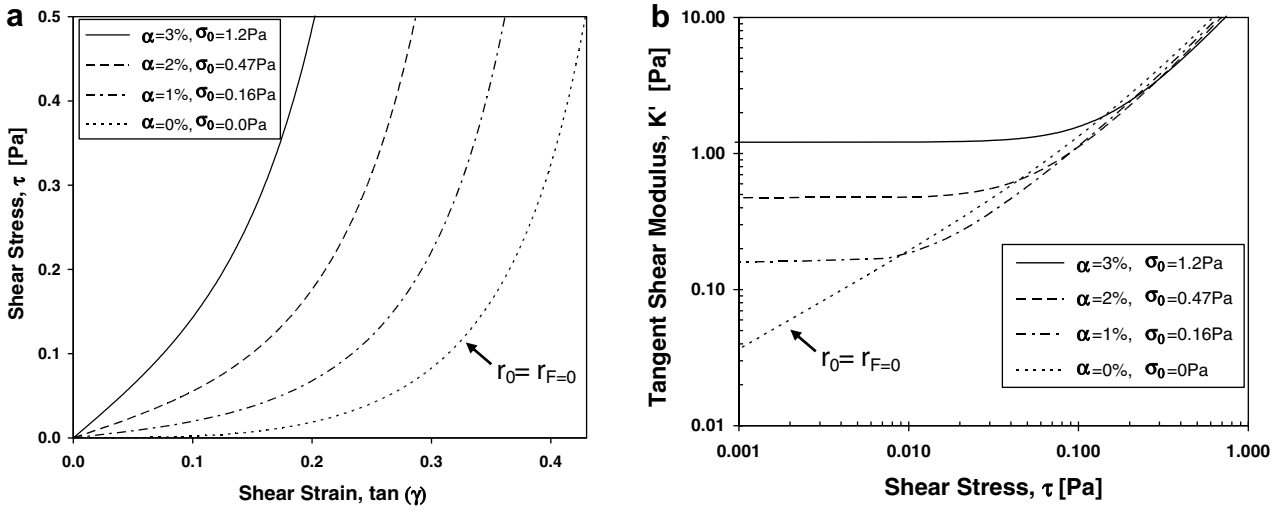

Fig. 10. Effect of network prestress on the network shear stress–shear strain behavior (a) and the network tangent modulus–shear stress behavior (b), with the initial prestress (σ_0) based on $r_0 = r_{F=0}(1 + \alpha)$.

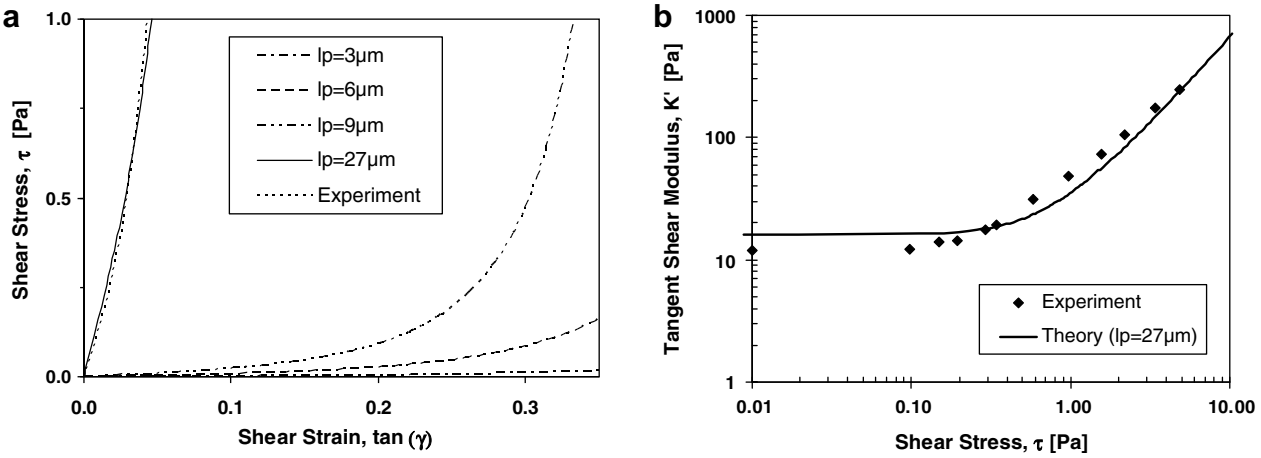

Fig. 12. (a) Shear stress–shear strain response and (b) tangent shear modulus–shear stress response of bundled F-actin networks with varying persistence length ($R = 0.5$, $c_{AF} = 7$ μM). The experimental data are adapted from Ref. [22].

Table 2
Network parameters for different amounts of filament bundling

m_{bonded} (no. per bundle)	$m_{unbonded}$ (no. per bundle)	$l_{p,m}$ (μm)	$r_{F=0}$ (μm)	r_0 (μm)	α (%)	R	c_{AF} (μM)	L_c (μm)	n (m^{-3})
1	1	3	1.81	1.83	1	0.5	7	2.04	5.4e18
2	2	6	1.92	1.94	1	0.5	7	2.04	5.4e18
–	3	9	1.96	1.98	1	0.5	7	2.04	5.4e18
3	9	27	2.01	2.03	1	0.5	7	2.04	5.4e18

is the radius of a single fiber) and the effective radius required for an equivalent cross-sectional area is $R_{eff} = \sqrt{m} r_s$. Since the area moment of inertia of a solid cylinder is $I = (\pi R_{eff}^4)/4$, the ratio of increasing effective stiffness for bonded bundled filaments can be calculated as follows (with E as Young's modulus):

$$\frac{l_{p,m}}{l_{p,s}} = \frac{\kappa_m}{\kappa_s} = \frac{(EI)_m}{(EI)_s} = \frac{(R_{eff})^4}{(r_s)^4} = m^2 \tag{13}$$

The results for scaling the persistence length of a single actin filament to obtain the effective persistence length, $l_{p,m}$, of a bonded bundle of m filaments are given in Fig. 12. Table 2 contains the network parameters used for each case in Fig. 12. Each actin network was taken to have a prestress set by assuming $\alpha = 1\%$, but with the persistence length increasing for increasing numbers of bundled filaments. The contour length was calculated using Eq. (12) with $d_{Actin} = 7$ nm and $c_{AF} = 7$ μM, resulting in $L_c = 2.04$ μm.

The case of $l_p = 6$ μm represents a bundle of two filaments while the case of $l_p = 3^2 \times 3 = 27$ μm represents a bonded bundle of three filaments. The smallest stable filament bonded bundle is assumed to consist of three filaments, and this case also exhibits excellent agreement with the experimental shear stress–strain data (Fig. 12a) as well as the tangent shear modulus–stress data of Gardel et al. (Fig. 12b).

Alternatively, if the model assumes linear scaling of bending stiffness due to unbonded bundles (Fig. 11b), then the same case ($R = 0.5$, $c_{AF} = 7$ μM) with three filaments would exhibit reduced stiffness, as shown by the $l_p = 9$ μm curve in Fig. 12a. Of course, the unbonded, bundled case matches the $R = 0.5$ data equally as well if nine filaments are bundled instead of three ($l_p = 9 \times 3 = 27$ μm). This unbonded bundle of nine filaments would have an average diameter ($D_B \sim 30$–40 nm, depending on the spacing between filaments) on the order of the actin–scruin bundle diameters observed by Shin et al. [4] via confocal microscopy ($D_B \sim 20$–65 nm for $R = 1$, with $D_B \sim R^{0.3}$). This would suggest that bundled actin fibers in the Gardel networks are only minimally bonded to each other for the case of $c_{AF} = 7$ μM, $R = 0.5$.

4. Concluding remarks

Constitutive models for F-actin microstructural network behavior have been created using single molecule models for individual filament force–extension behavior in conjunction with an eight-chain network model to capture the non-affine 3-D molecular network behavior. The single filament force–extension constitutive model was based on the MacKintosh derivation of the Kratky–Porod energy functional for semiflexible filaments ($l_p \sim L_c$). In further developing this model, we developed an accurate approximation for the MacKintosh force–extension expression of the form $F_{Mac} = \widehat{F}_{Mac}(r)$ using a Padé approximation. When combined with the eight-chain network model, the MacKintosh model was able to accurately capture the initial stiffness and nonlinear strain stiffening behavior observed in shear rheology experiments. The 3-D cytoskeletal network constitutive model presented provides the

ability to track microstructural stretch and orientation states under macroscopic stretching conditions in an averaged manner, and also enables variation of the filament mechanical properties and concentrations.

In Appendix A, an eight-chain network model considering a linear constitutive model of the filament force–extension behavior is presented and compared with the nonlinear MacKintosh model developed in the main text. The linear force–extension relationship was found to result in strain stiffening of the network, a consequence of filament rotation during network deformation. However, the evolution in stiffness with strain differed from the behavior seen in experiments, underscoring the need to also include nonlinear force–extension relationships for actin filaments.

Using the eight-chain MacKintosh network constitutive model, we examined the experimentally observed effects on the network stress–strain behavior that occur from increasing the actin concentration. The model's shear stress–shear strain response compares favorably with rheological data at low (8 and 12 μM) and high (29 μM) actin concentrations. The network model also exhibited good agreement with the experimental tangent modulus–shear stress data for $c_{AF} = 21$ μM in both the low and high stress regions, but not in the intermediate transition region. The experimental 21 μM data was shown to exhibit an anomalous, delayed transition to strain stiffening behavior in comparison to the other experimental concentration cases, which explained its diverging behavior from the theoretical prediction. The network model's prediction for the transition to strain stiffening behavior for the 21 μM case, however, did coincide with the trend exhibited by the other experimental concentration cases. The tangent shear moduli in the nonlinear strain stiffening region, often difficult to model, also correlate well with the data for all concentrations. This suggests that the network model is effectively simulating the cooperative network behavior and the accommodation of the shear strain through chain rotation and a small amount of end-to-end chain extension.

We parametrically varied the network prestress and network bundling to quantify their influence on network stress–strain behavior. Small increases in network prestress (α) produced large increases in initial network stiffness (G_0), with a constant relation between tangent shear modulus and shear stress for high stresses. We found an increase in network stiffness by increasing $l_{p,m}$, with excellent agreement between experimentally bundled actin networks ($R = 0.5$, $c_{AF} = 7$ μM) and the corresponding modeled networks composed of three-filament bundles. The overall constitutive framework enables predictions of large-strain multi-axial deformation of 3-D isotropic F-actin filament networks, and can be extended to model in vivo F-actin networks or in vitro networks of other filaments once updated with the proper material properties.

The proposed constitutive model provides a framework for the strain energy formulation to be extended to include the influence of cross-linking junction torsional potentials as well as enthalpic contributions from direct axial stretching of filaments, which will enable a simplified model and a future study on the tradeoffs between rotation vs. axial stretching as a means of microstructurally accommodating macroscopic deformation. The ability of the model to monitor the force at the cross-link junctions can also be utilized to explore effects of the rupture of cross-links at larger strains. Furthermore, the model provides an initial framework for including active remodeling of cytoskeletal networks, such as the actin network's reformulation in response to mechanical and chemical stimuli. A fully coupled 3-D cytoskeletal network model could be integrated with membrane and nucleus models in a finite element-based micromechanical model of the cell which would provide the ability to assign and evolve mechanical properties and filament concentrations as a function of location within the cell. Enhancements such as these could eventually lead to a composite cellular microstructural model that would enable detailed mechanical modeling of eukaryotic cells under a wide variety of loading conditions encountered during both healthy and diseased cellular functions.

Acknowledgements

J.S.P. is supported by Lincoln Laboratory through the Lincoln Doctoral Scholars Program under Air Force Contract No. FA8721-05-C-0002. The opinions, interpretations, recommendations and conclusions are those of the authors and are not necessarily endorsed by the US Government. M.C.B. acknowledges support from the Gail E. Kendall professorship.

Appendix A

A.1. Network stress–strain behavior using a nonlinear MacKintosh model in comparison with using a linear model for constituent filament force–extension behavior

Here we compare the network behavior obtained considering the constituent filaments to follow a linear force–extension behavior with that obtained when the chains exhibit the nonlinear force–extension behavior as represented in the main text with the MacKintosh model. This comparison will help highlight the source of nonlinearity in the network stress–strain behavior arising from the evolution in structure geometry due to chain rotation from that arising due to the nonlinearity of the filament behavior.

The force–extension relationship for the linear model is shown below, where k_{lin} is the linear stiffness of the filament

$$F_{\text{Linear}} = k_{\text{lin}}\boldsymbol{\delta} = k_{\text{lin}}(r - r_0) = k_{\text{lin}} r_0(\lambda_c - 1) \tag{14}$$

Fig. 13 compares the force—end-to-end distance and force—stretch behaviors of the MacKintosh and linear models using F-actin network properties (see Table 3 for values and discussion), with r_0 labeled for each model. Note in Fig. 13b that MacKintosh response (with $r_0 > r_{F=0}$) leads to an automatic chain pretension at $r = r_0$ ($\lambda_c = 1$).

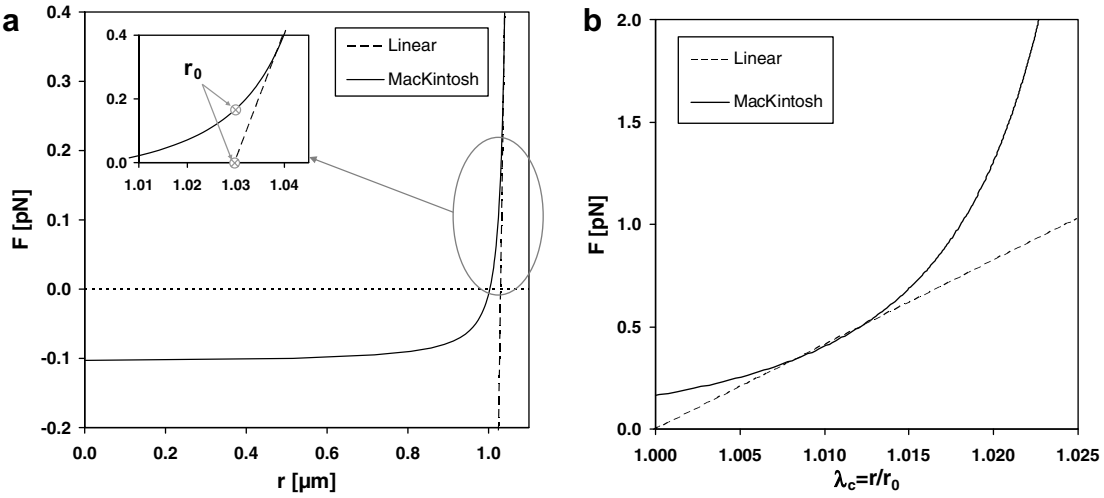

Fig. 13. (a) Force vs. end-to-end distance and (b) force vs. chain stretch behavior of F-actin filaments using the linear and MacKintosh models.

Table 3
Network parameters and material properties (MacKintosh and linear models)

	MacKintosh	Linear
n (filaments m^{-3})	1.2e19	1.2e19
Stiffness term	$l_p = 3.0$ μm	$k_{lin} = 40$ μN m^{-1}
L_c (μm)	1.07	1.07
r_0 (μm)	1.03	1.03
$r_{F=0}$ (μm)	1.00	1.03

The expressions for the strain energy density of the eight-filament cytoskeletal network models based on the linear and MacKintosh model are

$$U_{\text{Linear}} = nk_{\text{lin}}\left(\frac{r^2}{2} - rr_0 - c\right)$$
$$U_{\text{Mac}} = \frac{nk_BT}{l_p}\left[\frac{L_c}{4(1-r/L_c)} - l_p[\ln(L_c^2 - 2l_pL_c + 2l_pr) - \ln(r - L_c)] - c\right] \quad (15)$$

where c is a constant equal to the initial strain energy of the filament. Following the derivation of the Cauchy stress–strain relationship developed earlier for the MacKintosh model, the corresponding Cauchy shear stress–strain relationships for the three single filament models become

$$\tau_{\text{Linear}} = \frac{nk_{\text{lin}}r_0^2}{3}\left(1 - \frac{1}{\lambda_c}\right)\tan\gamma$$
$$\tau_{\text{Mac}}(r) = \frac{nk_BT}{3l_p}\frac{r_0}{\lambda_c}\left(\frac{1}{4(1-r/L_c)^2}\right) \times \left(\frac{L_c/l_p - 6(1-r/L_c)}{L_c/l_p - 2(1-r/L_c)}\right)\tan\gamma \quad (16)$$

A.2. Comparison with representative low concentration case

The models were evaluated by comparing the data with the lowest actin concentration ($c_{AF} = 8$ μM and $R = 0.03$) shown to exhibit network behavior [22]. The parameters

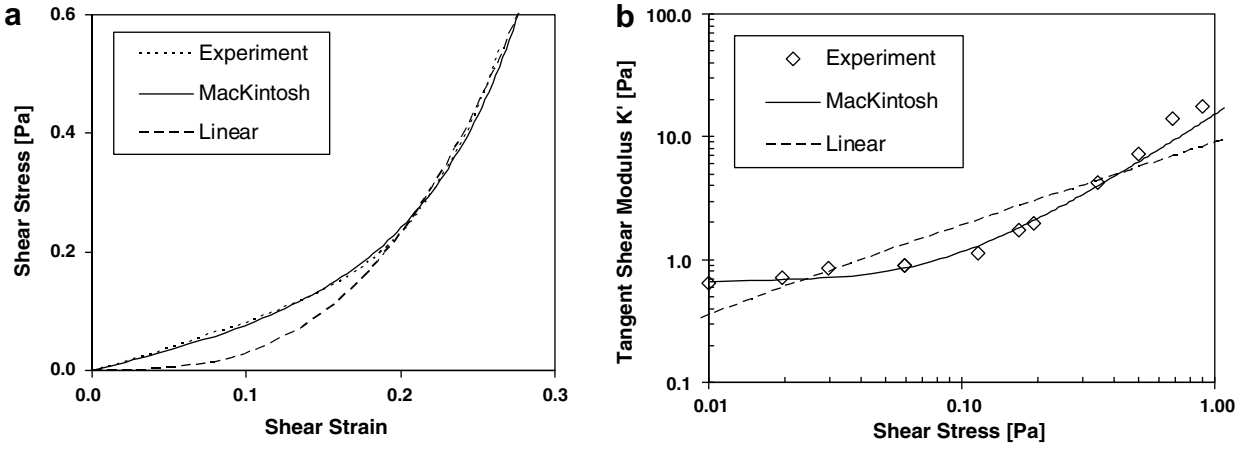

Fig. 14. (a) Shear stress–strain and (b) tangent shear modulus–shear stress for in vitro F-actin networks ($c_{AF} = 8$ μM, $R = 0.03$). The experimental data are from Ref. [22].

in Table 3 are used in the MacKintosh and linear network models.

The stiffness-related term (l_p or k_{lin}) and r_0 (via α) are chosen to best fit the models to the 8 μM experimental data. The shear stress–strain results are shown in Fig. 14a, with the tangent modulus–shear stress results shown in Fig. 14b. If the linear stiffness is related to actin filament geometry as $k_{lin} = AE/L_c = (AEI)/(L_c I) = (16 l_p k_B T)/(d_{AF}^2 L_c)$ with $d_{AF} = 7$ nm, then $l_p = 0.03$ μm for the best overall fit shown in Fig. 14a. This persistence length value is two orders of magnitude lower than experimentally observed F-actin values ($l_p \sim 3$–17 μm).

Note that the network with linear filaments exhibits a nonlinear network shear stress–shear strain behavior in Fig. 14a due to the filament rotation effects [34]. The linear model, however, captures neither the shear stress–strain nor the tangent modulus–stress behavior of the actin network, emphasizing the importance of using a nonlinear force–extension relationship for single F-actin filaments. The tangent modulus–stress response of the MacKintosh model, when used in an eight-chain network, closely matches the predictions given by Gardel et al. [22], with a good fit at low stresses as well as in the strain stiffening region at higher stresses (Fig. 14b). The eight-chain MacKintosh network model, because of its superior performance when compared with experimental data, was chosen for further comparison with actin networks at varying concentrations in the main text.

Appendix B

B.1. Network model performance with varying persistence length

Here we address the network model's ability to fit experimental data over a range of persistence lengths. As mentioned in the main text, there is a range of published values and testing methods for persistence lengths of in vitro actin filaments ($l_p \sim 3$–17 μm). We compare the model's behavior for $l_p = 3,\ 10,\ 17$ μm ($c_{AF} = 8.33$ μM,

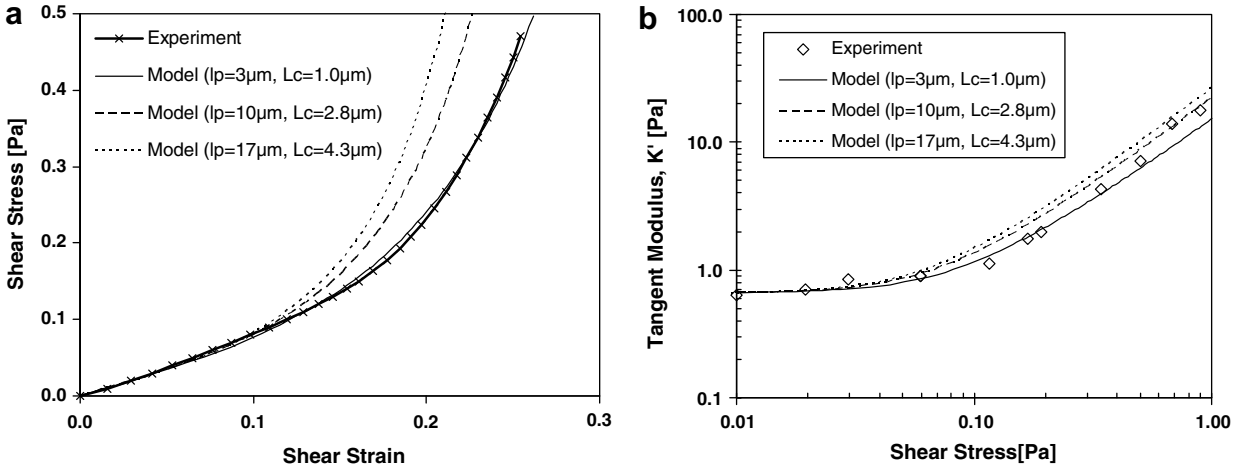

Fig. 15. (a) Shear stress–shear strain and (b) tangent shear modulus–shear stress for in vitro F-actin networks over the range of published persistence lengths $l_p = 3$, 10, 17 μm ($c_{AF} = 8$ μM, $R = 0.03$), varying L_c for best fit. The experimental data are from Ref. [22].

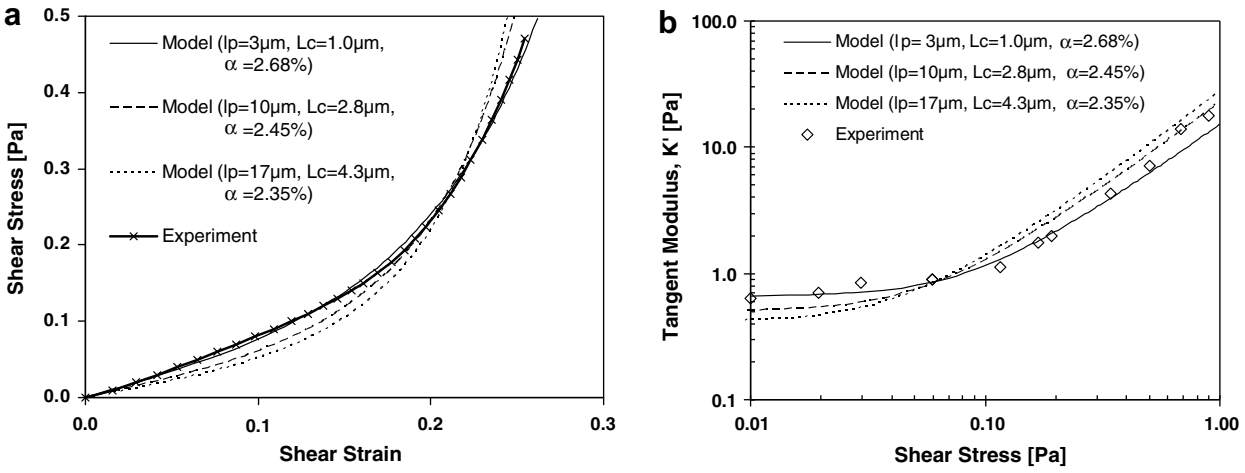

Fig. 16. (a) Shear stress–shear strain and (b) tangent shear modulus–shear stress for in vitro F-actin networks over the range of published persistence lengths $l_p = 3$, 10, 17 μm ($c_{AF} = 8$ μM, $R = 0.03$), varying L_c and α for best fit. The experimental data are from Ref. [22].

$R = 0.03$) by only varying L_c to obtain a best fit to the initial shear modulus (see Fig. 15).

In order to obtain a best fit to the data, an increase in the persistence length to 10 or 17 μm requires the contour length to be increased to $L_c = 2.8$, 4.3 μm, respectively, both of which are beyond experimentally observed values (i.e. $L_c \sim 1$ μm). Note that while the fit appears good in the tangent modulus–shear stress plot (with log–log axes) in Fig. 15b, the shear stress–strain plot in Fig. 15a reveals divergent behavior in the nonlinear strain stiffening region for larger persistence lengths. A better overall fit can be obtained by varying α as well as L_c, as seen in Fig. 16.

Decreasing α while holding the contour lengths constant (from Fig. 15) gives a better fit in the strain stiffening region at the expense of a poorer fit to the initial shear modulus. The model's performance with higher persistence lengths, however, still does not achieve as good of a fit to the 8.33 μM data as with the $l_p = 3$ μm. The persistence length has a significant effect on the transition to the strain stiffening region as the bends in the filaments are straightened out, which enables a better fit of the more compliant actin–scruin filaments with the lower value of l_p. Since the best fit was obtained with $l_p = 3$ μm and a realistic contour length of $L_c = 1.0$ μm, these values were used for further comparison in the main text.

References

[1] Boal DH. Mechanics of the cell. Cambridge: Cambridge University Press; 2002.

[2] Maniotis AJ, Chen CS, Ingber DE. Demonstration of mechanical connections between integrins, cytoskeletal filaments, and nucleoplasm that stabilize nuclear structure. Proc Natl Acad Sci USA 1997;94:849.

[3] Isambert H, Maggs AC. Dynamics and rheology of actin solutions. Macromolecules 1996;29:1036.

[4] Shin JH, Gardel ML, Mahadevan L, Matsudaira P, Weitz DA. Relating microstructure to rheology of a bundled and cross-linked F-actin network in vitro. Proc Natl Acad Sci USA 2004;101:9636.

[5] Gardel ML, Nakamura F, Hartwig JH, Crocker JC, Stossel TP, Weitz DA. Prestressed F-actin networks cross-linked by hinged filamins replicate mechanical properties of cells. Proc Natl Acad Sci USA 2006;103:1762.

[6] Janmey PA, Euteneuer U, Traub P, Schliwa M. Viscoelastic properties of vimentin compared with other filamentous biopolymer networks. J Cell Biol 1991;113:155.

[7] Fernandez P, Pullarkat PA, Ott A. A master relation defines the nonlinear viscoelasticity of single fibroblasts. Biophys J 2006;90:3796.

[8] Gittes F, Mickey B, Nettleton J, Howard J. Flexural rigidity of microtubules and actin filaments measured from thermal fluctuations in shape. J Cell Biol 1993;120:923.

[9] Isambert H, Venier P, Maggs AC, Fattoum A, Kassab R, Pantaloni D, et al. Flexibility of actin filaments derived from thermal fluctuations. Effect of bound nucleotide, phalloidin, and muscle regulatory proteins. J Biol Chem 1995;270:11437.

[10] Janmey PA, Hvidt S, Kas J, Lerche D, Maggs A, Sackmann E, et al. The mechanical properties of actin gels. Elastic modulus and filament motions. J Biol Chem 1994;269:32503.

[11] Wagner OI, Rammensee S, Korde N, Wen Q, Leterrier JF, Janmey PA. Softness, strength and self-repair in intermediate filament networks. Exp Cell Res 2007;313:2228.

[12] Hvidt S, Nestler FH, Greaser ML, Ferry JD. Flexibility of myosin rod determined from dilute solution viscoelastic measurements. Biochemistry 1982;21:4064.

[13] Ott A, Magnasco M, Simon A, Libchaber A. Measurement of the persistence length of polymerized actin using fluorescence microscopy. Phys Rev E Stat Phys Plasmas Fluids Relat Interdiscip Top 1993;48:R1642.

[14] Riveline D, Wiggins CH, Goldstein RE, Ott A. Elastohydrodynamic study of actin filaments using fluorescence microscopy. Phys Rev E 1997;56:R1330.

[15] Takebayashi T, Morita Y, Oosawa F. Electronmicroscopic investigation of the flexibility of F-actin. Biochim Biophys Acta 1977;492:357.

[16] Steinmetz MO, Goldie KN, Aebi U. A correlative analysis of actin filament assembly, structure, and dynamics. J Cell Biol 1997;138:559.

[17] Kasza KE, Rowat AC, Liu J, Angelini TE, Brangwynne CP, Koenderink GH, et al. The cell as a material. Curr Opin Cell Biol 2007;19:101.

[18] Gisler T, Weitz DA. Scaling of the microrheology of semidilute F-actin solutions. Phys Rev Lett 1999;82:1606.

[19] MacKintosh FC, Kas J, Janmey PA. Elasticity of semiflexible biopolymer networks. Phys Rev Lett 1995;75:4425.

[20] Storm C, Pastore JJ, MacKintosh FC, Lubensky TC, Janmey PA. Nonlinear elasticity in biological gels. Nature 2005;435:191.

[21] Xu JY, Schwarz WH, Kas JA, Stossel TP, Janmey PA, Pollard TD. Mechanical properties of actin filament networks depend on preparation, polymerization conditions, and storage of actin monomers. Biophys J 1998;74:2731.

[22] Gardel ML, Shin JH, MacKintosh FC, Mahadevan L, Matsudaira P, Weitz DA. Elastic behavior of cross-linked and bundled actin networks. Science 2004;304:1301.

[23] Gibson LJ, Ashby MF. Cellular solids: structure & properties. Oxford: Pergamon Press; 1988.

[24] Satcher Jr RL, Dewey Jr CF. Theoretical estimates of mechanical properties of the endothelial cell cytoskeleton. Biophys J 1996;71:109.

[25] Warren WE, Kraynik AM. Linear elastic behavior of a low-density Kelvin foam with open cells. J Appl Mech—Trans ASME 1997;64:787.

[26] Stamenovic D, Ingber DE. Models of cytoskeletal mechanics of adherent cells. Biomech Model Mechanobiol 2002;1:95.

[27] Landau LD, Lifshitz EM. Reading statistical physics, Part I. Course of theoretical physics, vol. 5. Reading, MA: Addison-Wesley; 1974.

[28] Kratky O, Porod G. Röntgenuntersuchung gelöster Fadenmoleküle. Rec Trav Chim Pays—Bas 1949;68:1106.

[29] Bustamante C, Marko JF, Siggia ED, Smith S. Entropic elasticity of lambda-phage DNA. Science 1994;265:1599.

[30] Marko JF, Siggia ED. Stretching DNA. Macromolecules 1995;28:209.

[31] Odijk T. Stiff chains and filaments under tension. Macromolecules 1995;28:7016.

[32] Smith SB, Cui Y, Bustamante C. Overstretching B-DNA: the elastic response of individual double-stranded and single-stranded DNA molecules. Science 1996;271:795.

[33] Wang MD, Yin H, Landick R, Gelles J, Block SM. Stretching DNA with optical tweezers. Biophys J 1997;72:1335.

[34] Arslan M, Boyce MC. Constitutive modeling of the finite deformation behavior of membranes possessing a triangulated network microstructure. J Appl Mech 2006;73:536.

[35] Arslan M, Boyce MC, Qi HJ, Ortiz C. Constitutive modeling of the stress–stretch behavior of two-dimensional triangulated macromolecular networks containing folded domains. J Appl Mech 2008;75:011020.

[36] Qi HJ, Ortiz C, Boyce MC. Mechanics of biomacromolecular networks containing folded domains. J Eng Mater Technol—Trans ASME 2006;128:509.

[37] MacKintosh FC. Theoretical models of viscoelasticity of actin solutions and the actin cortex. Biol Bull 1998;194:351.

[38] Treloar LRG, Riding G. A non-Gaussian theory for rubber in biaxial strain. I. Mechanical properties. Proc Roy Soc Lond. Ser A, Math Phys Sci 1979;369:261.
[39] Wu PD, van der Giessen E. On improved network models for rubber elasticity and their applications to orientation hardening in glassy-polymers. J Mech Phys Solids 1993;41:427.
[40] Li J, Dao M, Lim CT, Suresh S. Spectrin-level modeling of the cytoskeleton and optical tweezers stretching of the erythrocyte. Biophys J 2005;88:3707.
[41] Dao M, Li J, Suresh S. Molecularly based analysis of deformation of spectrin network and human erythrocyte. Mater Sci Eng C 2006;26:1232.
[42] Li J, Lykotrafitis G, Dao M, Suresh S. Cytoskeletal dynamics of human erythrocyte. PNAS 2007;104:4937.
[43] Arruda EM, Boyce MC. A three-dimensional constitutive model for the large stretch behavior of rubber elastic materials. J Mech Phys Solids 1993;41:389.
[44] MacKintosh FC. Polymer-based models of cytoskeletal networks. In: Mofrad MK, Kamm RD, editors. Cytoskeletal mechanics: models and measurements. Cambridge: Cambridge University Press; 2006.
[45] Cohen A. A Padé approximant to the inverse Langevin function. Rheol Acta 1991;30:270.
[46] Bergstrom JS, Boyce MC. Deformation of elastomeric networks: relation between molecular level deformation and classical statistical mechanics models of rubber elasticity. Macromolecules 2001;34:614.
[47] Arruda EM, Boyce MC. Evolution of plastic anisotropy in amorphous polymers during finite straining. Int J Plast 1993;9:697.
[48] Bischoff JE, Arruda EM, Grosh K. Orthotropic hyperelasticity in terms of an arbitrary molecular chain model. J Appl Mech 2002;69:198.
[49] Kuhl E, Garikipati K, Arruda EM, Grosh K. Remodeling of biological tissue: mechanically induced reorientation of a transversely isotropic chain network. J Mech Phys Solids 2005;53:1552.
[50] Bertoldi K, Boyce MC. Mechanics of the hysteretic large strain behavior of mussel byssus threads. J Mater Sci 2007;42:8943.
[51] Chandran PL, Barocas VH. Affine versus non-affine fibril kinematics in collagen networks: theoretical studies of network behavior. J Biomech Eng 2006;128:259.
[52] Onck PR, Koeman T, van Dillen T, van der Giessen E. Alternative explanation of stiffening in cross-linked semiflexible networks. Phys Rev Lett 2005;95:178102.
[53] Wang N, Tolic-Norrelykke IM, Chen J, Mijailovich SM, Butler JP, Fredberg JJ, et al. Cell prestress. I. Stiffness and prestress are closely associated in adherent contractile cells. Am J Physiol Cell Physiol 2002;282:C606.
[54] Zhu C, Bao G, Wang N. Cell mechanics: mechanical response, cell adhesion, and molecular deformation. Ann Rev Biomed Eng 2000;2:189.
[55] Gardel ML, Shin JH, MacKintosh FC, Mahadevan L, Matsudaira PA, Weitz DA. Scaling of F-actin network rheology to probe single filament elasticity and dynamics. Phys Rev Lett 2004;93:188102.
[56] Janmey PA, McCormick ME, Rammensee S, Leight JL, Georges PC, Mackintosh FC. Negative normal stress in semiflexible biopolymer gels. Nature Mater 2007;6:48.
[57] Bischoff JE, Arruda EA, Grosh K. A microstructurally based orthotropic hyperelastic constitutive law. J Appl Mech 2002;69:570.
[58] Niederman R, Amrein PC, Hartwig J. Three-dimensional structure of actin filaments and of an actin gel made with actin-binding protein. J Cell Biol 1983;96:1400.